

# CONSTRAINTS ON THE SURFACE MAGNETIC FIELDS AND AGE OF A COOL HYPERGIANT: XMM-NEWTON X-RAY OBSERVATIONS OF VY CMA

RODOLFO MONTEZ JR.

Department of Physics and Astronomy, Vanderbilt University, Nashville, TN 37235, USA

JOEL H. KASTNER

Center for Imaging Science, School of Physics and Astronomy, and Laboratory for Multiwavelength Astrophysics, Rochester Institute of Technology, 54 Lomb Memorial Drive, Rochester, NY 14623, USA

ROBERTA M. HUMPHREYS

Minnesota Institute for Astrophysics, 116 Church Street SE, University of Minnesota, Minneapolis, MN 55455, USA

REBECCA LEIGH TUROK

Vanderbilt University, Nashville, TN 37235, USA

KRIS DAVIDSON

Minnesota Institute for Astrophysics, 116 Church Street SE, University of Minnesota, Minneapolis, MN 55455, USA

*Accepted by the Astrophysical Journal*

## ABSTRACT

The complex circumstellar ejecta of highly evolved, cool hypergiants are indicative of multiple, asymmetric mass loss events. To explore whether such episodic, non-isotropic mass loss may be driven by surface magnetic activity, we have observed the archetypical cool hypergiant VY Cma with the XMM-Newton X-ray satellite observatory. The hypergiant itself is not detected in these observations. From the upper limit on the X-ray flux from VY Cma at the time of our observations ( $F_{X,UL} \approx 8 \times 10^{-14}$  erg cm<sup>-2</sup> s<sup>-1</sup>, corresponding to  $\log L_X/L_{bol} \leq -8$ ), we estimate an average surface magnetic field strength  $fB \leq 2 \times 10^{-3}$  G (where  $f$  is the filling factor of magnetically active surface regions). These X-ray results for VY Cma represent the most stringent constraints to date on the magnetic field strength near the surface of a hypergiant. VY Cma's mass loss is episodic and may have been in a state of low surface magnetic activity during the XMM observations. The XMM observations also yield detections of more than 100 X-ray sources within  $\sim 15'$  of VY Cma, roughly 50 of which have near-infrared counterparts. Analysis of X-ray hardness ratios and IR colors indicates that some of these field sources may be young, late-type stars associated with VY Cma, its adjacent molecular cloud complex, and the young cluster NGC 2362. Further study of the VY Cma field is warranted, given the potential to ascertain the evolutionary timescale of this enigmatic, massive star.

*Subject headings:* stars: individual: VY Cma (HD 58061); X-rays: stars; stars: early-type; stars: magnetic field; stars: pre-main sequence

## 1. INTRODUCTION

High-resolution imaging of the cool, rapidly mass-losing hypergiants<sup>1</sup> VY Cma and IRC+10420 have yielded evidence for multiple, asymmetric mass loss events (Humphreys et al. 1997; Smith et al. 2001; Humphreys et al. 2002, 2005, 2007; Tiffany et al. 2010). These stars are the most luminous known for their apparent photospheric temperatures, and their mass loss rates rank among the highest for cool stars (i.e., a few  $\times 10^{-4}$  M<sub>⊙</sub> yr<sup>-1</sup>). It has been suggested (Smith et al. 2001; Humphreys et al. 2005, 2007; Tiffany et al. 2010) that the complex loops, arcs and knots in their ejecta are possibly due to strong surface magnetic activity. Recent ALMA observations of VY Cma, which reveal distinct, asymmetrically distributed clumps of ejecta on scales

of tens of stellar radii, further reinforce such a notion (O’Gorman et al. 2014).

Indeed, the presence of starspots, as manifest by large surface brightness anisotropies, has been inferred for several cool supergiants. The best-studied example is  $\alpha$  Ori (Gilliland & Dupree 1996), but stellar hotspots have also been observed on  $\alpha$  Sco and  $\alpha$  Her with properties consistent with a convective, hence magnetic, origin (Tuthill et al. 1997). Interferometric imaging of cool hypergiant stars reveals large-scale inhomogeneities attributed to magnetic fields and/or rotation (Monnier et al. 2004). Magnetic fields have now been measured in the ejecta of several cool hypergiant stars (Vlemmings et al. 2002, 2005), lending support to the notion that their episodic mass loss may be driven by surface magnetic activity.

For rapidly mass-losing evolved stars, the potential connection between such magnetic activity and coronal X-ray emission remains to be established. Lumi-

<sup>1</sup> We use the term hypergiant to refer to evolved stars with spectral types from late A to M that lie just below the upper luminosity boundary in the HR Diagram.

nous X-ray emission from coronae associated with luminous red giants and supergiants is rarely observed (Ayres et al. 2003; Ayres 2005). However, there exists a dearth of meaningful measurements of the most rapidly mass-losing evolved stars; to assess the X-ray activity levels of such stars requires deep observations with adequate hard ( $\gtrsim 1$  keV) X-ray sensitivity to penetrate their thick circumstellar envelopes.

The mass loss asymmetries that develop during the very late stages in the evolution of massive stars are analogous to those that characterize stars on the asymptotic giant branch (AGB), post-AGB stars, and the very youngest planetary nebulae (PNe). Only a few such cool, rapidly mass-losing AGB and post-AGB stars have been observed by the two contemporary X-ray observatories that are well-suited to such work (i.e., Chandra and XMM-Newton). In XMM observations, the single, mass-losing AGB stars TX Cam and T Cas were not detected (Kastner & Soker 2004a) whereas Mira AB — a wide-separation AGB star and white dwarf (WD) binary that drives a large-scale bipolar outflow (Meaburn et al. 2009) — is quite luminous in X-rays (Kastner & Soker 2004b). Chandra imaging further revealed that both components of the Mira AB binary system are X-ray-luminous, and that Mira A (the AGB star) evidently undergoes energetic flaring (Karovska et al. 2005). The two additional known examples of X-ray-emitting AGB stars are also likely binary systems (Ramstedt et al. 2012). Meanwhile, Chandra observations are establishing that a significant fraction of the central stars of planetary nebulae are X-ray sources; as for AGB stars, these planetary nebula central star X-ray sources are frequently (though not exclusively) associated with binarity (Montez et al. 2010; Kastner et al. 2012; Freeman et al. 2014; Montez et al. 2014).

Moving higher on the HR diagram, only a few X-ray observations of supergiants and hypergiants have been obtained with modern X-ray observatories: the iconic red supergiant  $\alpha$  Ori is apparently “dark” in X-rays (Posson-Brown et al. 2006), and the yellow hypergiant IRC+10420 was not detected by XMM (De Becker et al. 2014).

Here, we report on a search for X-ray evidence of magnetic activity at VY CMa (HD 58061), via XMM-Newton observations. VY CMa is a special case even among the cool hypergiants. A powerful infrared and maser source, it is one of the most luminous and largest evolved cool stars known, and features one of the highest measured mass loss rates among evolved stars ( $2\text{--}3 \times 10^{-4} M_{\odot} \text{ yr}^{-1}$ ; Danchi et al. 1994). The star is surrounded by a complex, asymmetric dust reflection nebula  $10''$  in extent (Herbig 1972; Kastner & Weintraub 1998; Smith et al. 2001); this dusty circumstellar material obscures the central star across the visible wavelength range (Kastner & Weintraub 1998). Visual imaging, spectroscopy, and polarimetry (Smith et al. 2001; Humphreys et al. 2005, 2007; Jones et al. 2007) reveal that the nebula’s expanding arcs, prominence-like loops and knots were ejected at different times and in different directions, apparently by localized processes from different regions on the star.

As argued in Vlemmings et al. (2002), measurements of polarization from masers in the ejecta of VY CMa ap-

pear to trace a magnetic field that increase with strength moving closer to the surface of VY CMa. At large distances from the star ( $\sim 2800$  AU), OH maser polarization suggests a field strength of  $\sim 2$  mG (Cohen et al. 1987); at  $\sim 200$  AU, H<sub>2</sub>O maser polarization suggests 200 mG (Vlemmings et al. 2002); and, nearest the star, SiO maser polarization suggests a field strength of 65 G (Barvainis et al. 1987). This trend in the magnetic field strength from maser polarization is suggestive of a global field strength that drops like  $r^{-2}$ . Extrapolating this radial dependence implies that magnetic field strengths on the order of  $10^2$  to  $10^3$  G may exist at the surface of VY CMa.

To determine whether such strong magnetic fields might manifest themselves in the form of coronal X-ray activity, we used XMM to search for X-ray emission from VY CMa. These X-ray observations have the additional benefit that they can be used to assess whether the larger environment around VY CMa — which includes a large molecular cloud and the young stellar cluster NGC 2362 (Figure 1; Lada & Reid 1978) — might be populated by late-type, pre-main sequence stars that formed during the same episode of star formation that spawned the hypergiant itself. Such young, lower-mass stars should feature high levels of coronal activity and, hence, relatively large X-ray luminosities (e.g., Damiani et al. 2006).

## 2. DATA AND ANALYSIS

### 2.1. Observations

VY CMa was observed by the XMM-Newton satellite observatory on 07 May 2012 (ObsID: 0691190101). X-ray data were obtained with the European Photon Imaging Camera (EPIC), which is comprised of three X-ray imaging spectrometers (pn, MOS1, MOS2), and the X-ray dispersion grating spectrometers (RGS). Optical/UV imaging was performed with the optical monitor (OM) through visible (V;  $\lambda_{\text{eff}} = 543$  nm) and ultraviolet filters (UVW1;  $\lambda_{\text{eff}} = 291$  nm). EPIC images were performed with the THICK optical blocking filter to ensure optical photons from VY CMa would not lead to a spurious detection. The EPIC detectors provide sensitivity in the 0.15 to 12 keV energy range with moderate energy resolution ( $E/\Delta E \sim 20\text{--}50$ ) at spatial resolution (point spread function core FWHM) of up to  $\sim 6\text{--}12''$ , albeit with broad half-encircled-energy widths up to  $15''$ . EPIC detectors pn, MOS1, and MOS2 were exposed for 20.0, 21.6, and 21.6 ks, respectively. The RGS and the OM data are unusable for our purposes due to lack of source photon detections and artifacts caused by the optical brightness of VY CMa, respectively. The apparent detection of VY CMa in the observation with the UVW1 filter is spurious and caused by residual charge from the saturated V filter observation. Hence, we focus our analysis on the EPIC observations and, in particular, on the pn data, as the pn instrument has the highest sensitivity over the energy range of X-ray emission expected from stellar coronal activity (i.e., a thermal plasma at temperatures of a few  $10^6$  K to a few  $10^7$  K).

We used the XMM-Newton pipeline products for our analysis. These Processing Pipeline System (PPS) products include “cleaned” event lists for the EPIC instruments; lists of X-ray sources detected in the field (via the PPS automated source detection routine); and X-

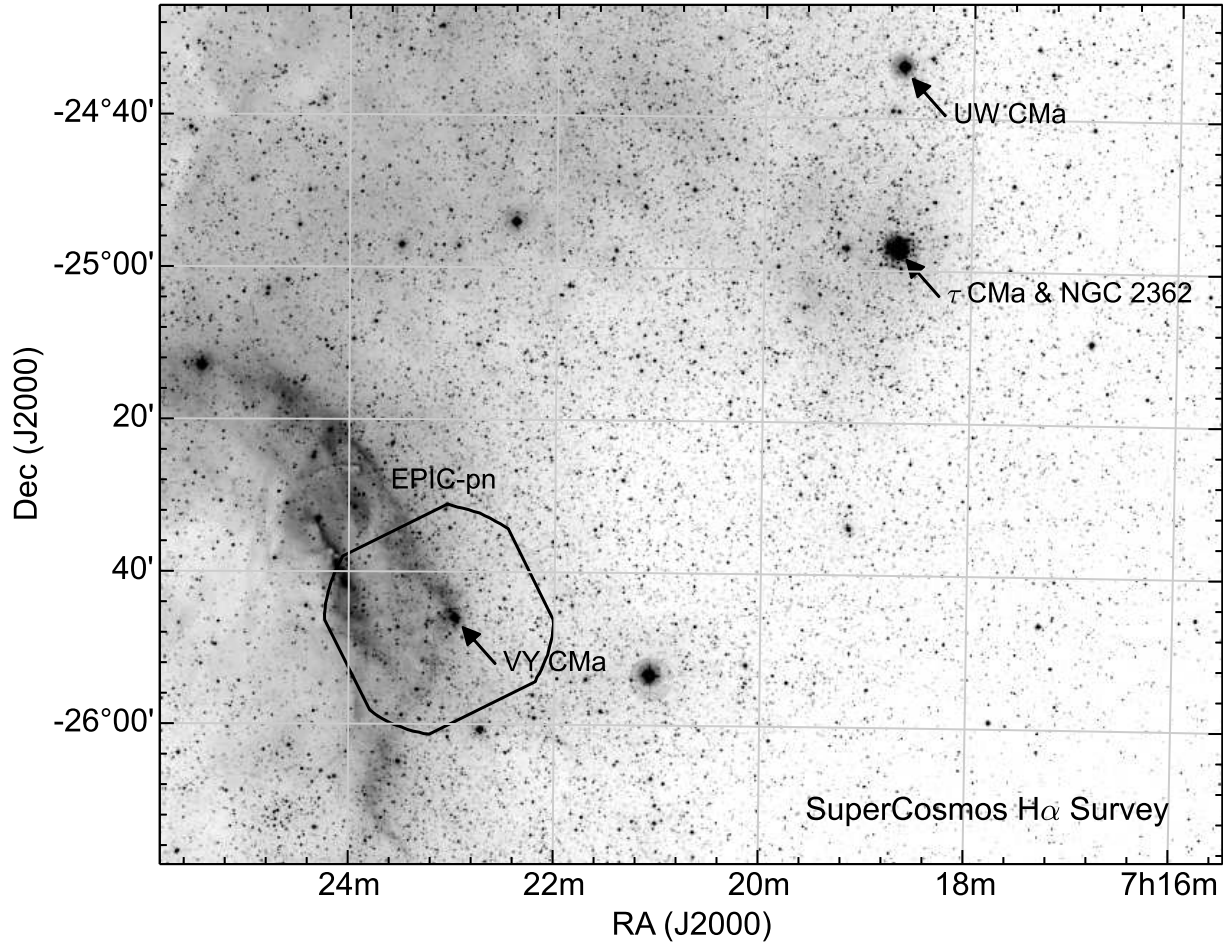


**Figure 1.** H- $\alpha$  image mosaic of a  $2.3 \times 1.8$  square degree field encompassing VY CMa, NGC 2362, and the semidetached eclipsing binary UW CMa, constructed from images acquired by the SuperCOSMOS H- $\alpha$  Survey (Parker et al. 2005). The field of the XMM-Newton EPIC-pn observation analyzed in this paper is indicated.

ray spectra and light curves for sources with at least 500 total-band EPIC counts, PSF-weighted detector coverage better than 50%, and total-band detection likelihood  $\geq 15$  (Watson et al. 2009). The PPS processing identified 20 X-ray emitting field sources in the vicinity (within  $\sim 5'$ ) of VY CMa and 107 in the entire field of view. The PPS product source lists include count rates determined within soft (S), medium (M), and hard (H) bands defined over the energy ranges 0.5-1.0 keV, 1.0-2.0 keV, and 2.0-4.5 keV, respectively. Two hardness ratios are calculated from these three bands,  $HR1 = (M-S)/(M+S)$ , and  $HR2 = (H-M)/(H+M)$ , and are used in our analysis (§2.3).

## 2.2. Limits on the X-ray flux from VY CMa

We constructed images within various energy bands (0.5-8.0 keV, 0.5-1.0 keV, 1.0-2.0 keV, 2.0-4.0 keV) to limit background, but found no evidence for X-ray emission from VY CMa in any of these images. We also extracted source and background spectra to search for spectroscopic evidence of X-ray emission from VY CMa. Five source-free circular regions, each with a radius of  $20''$  and restricted to the pn CCD containing VY CMa (i.e., CCD\_ID=7), were selected to define the background. The background-subtracted spectrum does not reveal any signal above the background. We conclude that VY CMa

is not detected in the EPIC observations.

To quantify the X-ray nondetection of VY CMa, we have estimated the source count rate required to produce a  $2\sigma$  detection above the background in the EPIC-pn observation. The background count rate is determined by extracting the counts in the aforementioned background regions. Within the energy range 0.5-8.0 keV, we found a total of 197 background counts from these five regions, for a normalized background count rate of  $1.57 \times 10^{-6}$  counts  $s^{-1}$  arcsecond $^{-2}$ . Scaling this background rate to a source region at RA [J2000] = 07:22:58.33, Dec [J2000] = -25:46:03.24 with a radius of  $30''$ , we predict  $89 \pm 9$  background counts at the position of VY CMa, consistent with the measured background of  $91 \pm 9$  counts at this position. Hence, we confirm the lack of detection of VY CMa in the XMM observation. The background-subtracted count rate required to produce a  $2\sigma$  detection in the 0.5 to 8 keV energy range is  $1.13 \times 10^{-3}$  counts  $s^{-1}$ , after correcting for the encircled energy fraction of 80% expected for the  $30''$  extraction region on the EPIC-pn observation.

To determine the sensitivity to X-ray flux corresponding to this background-subtracted  $2\sigma$  count rate, we must assume an underlying model. We hence adopt

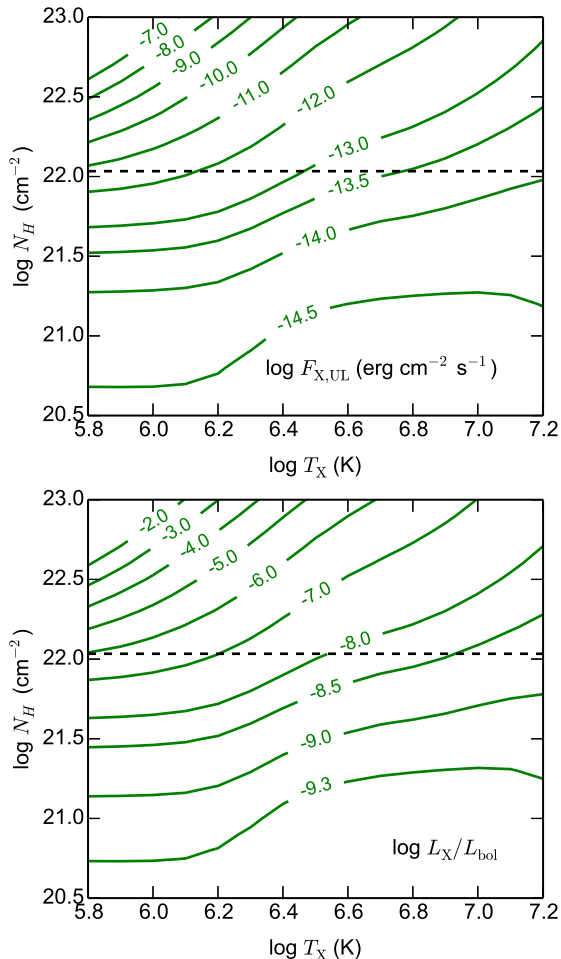


**Figure 2.** Upper limit calculations on the  $N_H$ – $T_X$  plane obtained from our XMM EPIC-pn observation of VY CMa. The contours indicate upper limits on source flux  $F_{X,UL}$  (top) and relative X-ray luminosity  $L_X/L_{bol}$  (bottom). The vertical dashed lines in each panel indicates the total (interstellar and circumstellar) absorption based on the visual extinction (Humphreys et al. 2007).

an absorbed, optically-thin thermal plasma (MEKAL; Mewe et al. 1985, 1986; Kaastra 1992; Liedahl et al. 1995) that effectively describes a variety of physical processes, including coronal activity and shocks in a stellar wind. For generality, we have computed X-ray fluxes for a grid of absorbing columns,  $N_H$ , and plasma temperatures,  $T_X$ , that covers a wide range of values ( $\log N_H[\text{cm}^{-2}] = 20$  to 23 and  $\log T_X[\text{K}]$  from 5.75 to 7.25). Lower temperatures are typical of solar-like coronal activity while the higher temperatures are typical of more energetic flare-like activity associated with coronal mass ejections (Orlando et al. 2004). Additionally, X-ray emission from wind shocks associated with early-type massive stars is typically characterized by plasma temperatures of a few  $10^6$  K and lower ISM absorbing columns (Nazé et al. 2011). We perform PIMMS simulations over the entire  $N_H$ – $T_X$  grid to estimate the  $2\sigma$  upper limit on X-ray flux,  $F_{X,UL}$ , from the  $2\sigma$  background-subtracted count rate. Assuming a distance of 1.3 kpc and  $L_{bol} \sim 3 \times 10^5 L_\odot$ , we then calculated upper limits for  $L_X/L_{bol}$ , a quantity often used as a stellar magnetic activity indicator. The results of these simulations are presented in Figure 2.

The total interstellar and circumstellar visual extinction,  $A_V$ , to VY CMa is estimated by Humphreys et al. (2007) as 5–6 mag. This suggests an intervening absorbing column of  $\sim 10^{22} \text{ cm}^{-2}$ . For such a column, at a nominal  $T_X$  of  $3 \times 10^6$  K, we estimate an unabsorbed  $F_{X,UL} = 8 \times 10^{-14} \text{ erg cm}^{-2} \text{ s}^{-1}$ ,  $L_X < 1.6 \times 10^{31} \text{ erg s}^{-1}$ , and  $\log L_X/L_{bol} < -8$ .

### 2.3. Classification of the X-ray Sources within the XMM Observation Field of View

We have cross-referenced all 107 X-ray sources detected in our XMM observation of VY CMa with infrared and astrometric catalogs: Two-Micron All Sky Survey Point Source Catalog (2MASS; Skrutskie et al. 2006), Wide-field Infrared Survey Explorer source catalog (WISE; Wright et al. 2010), and the United States Naval Observatory CCD Astrograph Catalog (UCAC4; Zacharias et al. 2013). The positional uncertainties of most these X-ray sources, according to the PPS output, is less than  $\sim 3''$ . Hence, we have identified potential IR counterparts for the PPS-identified X-ray sources using a correlation radius of  $6''$  and selecting the closest match to the position of the X-ray source. Within this correlation radius, we find 47 X-ray sources have potential IR counterparts. Ultimately, we dismissed the WISE point source data because VY CMa saturated the field with stray light. This stray light contamination is especially problematic at the longest WISE wavelengths.

We examined the total band detection likelihood (PN\_DET\_ML) as determined by the PPS source-detection algorithm to filter the source list to the most significant detections. We required that  $\text{PN\_DET\_ML} \geq 20$ , resulting in a sample of 43 well-detected X-ray sources, 27 of which have potential IR counterparts. The subsamples of these 43 X-ray sources with and without IR counterparts are illustrated in Figure 3 and are described in Tables 1 & 2, respectively.

At the distance to VY CMa (1.3 kpc), any source with a reliable measurement of proper motion is unlikely to be associated with the hypergiant. We identify nine IR counterparts among the 27 X-ray sources with potential IR counterparts that display evidence for significant (measurable) proper motions. Specifically, for each of these nine sources, the magnitude of proper motion error is less than 68% of the magnitude of the proper motion measurement itself. We do not consider these nine objects with significant proper motions further in this paper.

## 3. DISCUSSION

### 3.1. Constraints on the magnetic activity of VY CMa

Circular polarization measurements of masers around mass-losing AGB stars and supergiants provide estimates of magnetic fields at various displacements from the stars that are determined by the formation and survival of the observed molecules (Vlemmings et al. 2002, 2005). In many of these evolved star envelopes, the ensemble of masers at various radii from the star  $r$  suggests that the magnetic field strength  $B$  drops off as  $r^{-2}$  or  $r^{-3}$ , indicative of a solar-like or dipole-like magnetic field, respectively. The circular polarization measurements of VY CMa indicate that the magnetic field configuration may follow a solar-like magnetic field topology (see Figure 4),

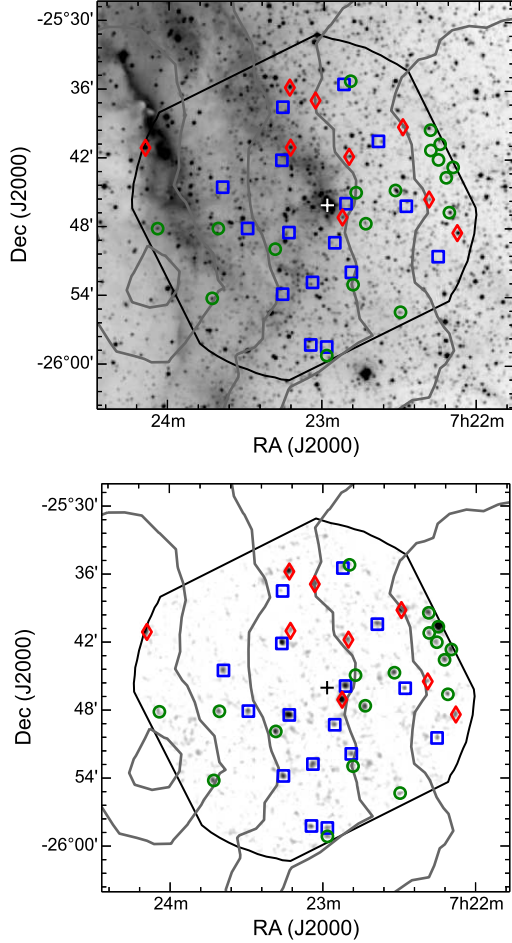


**Figure 3.** SuperCOSMOS H- $\alpha$  image (top) and XMM-Newton EPIC pn X-ray 0.5–8.0 keV image (bottom) of the VY CMa field. In each image, we have indicated the position of VY CMa by a cross and X-ray sources from the XMM observations by open symbols. Green circles indicate X-ray sources with IR counterparts, red diamonds are X-ray sources with significant proper motions, and blue squares are X-ray sources without IR counterparts. Contours corresponding to  $E_{B-V} = 0.5, 0.6, 1.0, 2.0$ , and 3.0 mag from the galactic extinction map of Schlegel et al. (1998) are represented by grey contours with extinction generally increasing from right to left.

which suggests the surface magnetic field strength could be  $\sim 200$  G. The total surface magnetic flux,  $\Phi_M$ , is given by  $\Phi_M = 4\pi R^2 f B$ , where the filling factor,  $f$ , parameterizes how  $\Phi_M$  is diluted by the relative size of the active areas on the surface. For a stellar radius appropriate for VY CMa and an arbitrary filling factor, the expected surface magnetic flux is then

$$\Phi_M = 2 \times 10^{26} \text{ Mx} \left( \frac{f}{10^{-5}} \right) \left( \frac{B}{200 \text{ G}} \right) \left( \frac{R}{1400 R_\odot} \right)^2, \quad (1)$$

where Mx is the maxwell unit ( $1 \text{ Mx} = 1 \text{ G cm}^2$ ).

To compare this estimate to our upper limit on the X-ray luminosity, we use an empirical relationship between stellar X-ray luminosity,  $L_X$  and magnetic flux,  $\Phi_M$ , that is found to hold over several orders of magnitude (Pevtsov et al. 2003). We caution that this relationship describes the behavior of active regions on the Sun and late-type stars and, hence, it is not clear if the same relationship would apply to magnetically-driven coronal

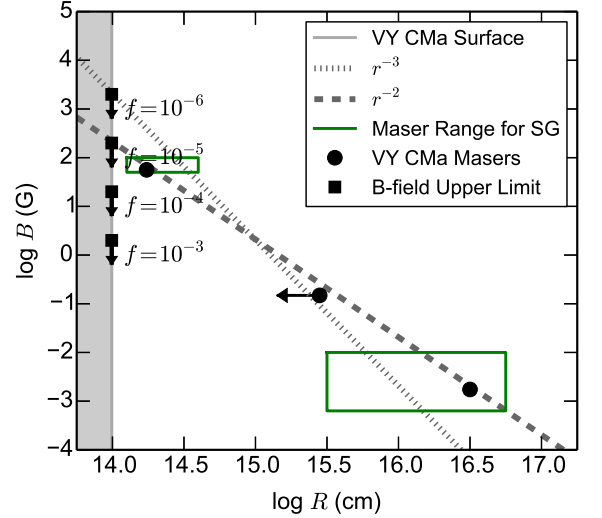


**Figure 4.** The limits on the surface magnetic field strength of VY CMa as determined from our XMM X-ray non-detection. The surface magnetic field strength upper limits determined from our non-detection of X-ray emission,  $\log L_X/L_{\text{bol}} = -8$  found by assuming  $\log N_H(\text{cm}^{-2}) = 22$  and  $\log T_X(K) = 6.5$  are overlaid for a few filling factors,  $f$ . We show magnetic field strengths inferred from maser measurements (see Vlemmings et al. 2002), the radial behavior for a solar-like ( $r^{-2}$ ) and dipole-like ( $r^{-3}$ ) magnetic field. The ranges of magnetic fields from maser measurements of all supergiants are shown by the green boxes.

activity on a supergiant. Feiden & Chaboyer (2013) provide a recent update of this relationship that is constrained by the largest number of low-mass stellar luminosity and magnetic field measurements to date; specifically,

$$\log \Phi_M = (11.86 \pm 0.68) + (0.459 \pm 0.018) \log L_X. \quad (2)$$

With their formulation, our upper limit on  $L_X$  of  $2 \times 10^{31} \text{ erg s}^{-1}$  — which is based on Figure 2 for  $\log T_X(K) = 6.5$  and  $\log N_H(\text{cm}^{-2}) = 22$  — suggests  $\Phi_M \lesssim 2 \times 10^{26} \text{ Mx}$ . We remark that for  $\log N_H(\text{cm}^{-2}) > 22$  and  $\log T_X(K) = 6.5$ , the upper limit on  $L_X$  becomes proportional to  $N_H^{2.8}$ , whereas  $\Phi_M \propto N_H^{1.4}$ ; hence, where inferred upper limits are concerned, the value for  $\Phi_M$  is less sensitive than  $L_X$  to the value adopted for  $N_H$ .

Overall, based on these considerations, the upper limit on the X-ray luminosity suggests that  $fB \lesssim 2 \times 10^{-3} \text{ G}$  for VY CMa. In Figure 4 we illustrate the surface magnetic field strength upper limits for various choices of filling factor  $f$ . Note that, adopting the maser-based estimate for the surface magnetic field, our X-ray upper limit indicates that  $f \lesssim 10^{-5}$ . Such an active region size is still substantial, given the enormous surface area of VY CMa; indeed, this filling factor upper limit corresponds to an active region comparable in size to the Earth-facing surface of a star with a radius of  $4R_\odot$ .

In the absence of constraints on the sizes of potential active regions on VY CMa, it is impossible to break the foregoing degeneracy between  $f$  and  $B$ . We note, however, that the presence of active regions is suggested by interferometric measurements that yield evidence for bright spots on the disks of a few red supergiants (Tuthill et al. 1997). In these objects, the bright spots have likely filling factors of a few tenths, which would suggest a low surface field strength assuming VY CMa is characterized by the same regime of  $f$ . On the

other hand, the episodic nature of the mass loss events from VY CMa is suggestive of periods of intense magnetic activity that generate eruptions. These eruptive events could be analogous to coronal mass ejections during periods of high solar activity, but with typical active-period timescales of decades rather than years (e.g., O’Gorman et al. 2014). Our X-ray nondetection could then indicate that VY CMa is not presently in such a magnetically active state.

### 3.2. X-ray Observations of Hypergiants

The yellow hypergiant IRC+10420 is the only other hypergiant that has been targeted thus far by a modern X-ray observatory. The non-detection of X-ray emission from IRC+10420 based on XMM-Newton observations was reported in De Becker et al. (2014). However, these authors report upper limits on the *observed* X-ray flux ( $\lesssim 1\text{--}3 \times 10^{-14}$  erg cm $^{-2}$  s $^{-1}$ ); as a result, their inferred relative source X-ray flux ( $f_X/f_{\text{bol}} \lesssim 1.1\text{--}3.5 \times 10^{-8}$ ) does not take into account the affects of intervening absorption. The large distance to IRC+10420 ( $D \sim 5$  kpc Jones et al. 1993) results in large interstellar absorption ( $A_V \sim 6$  mag), which dominates the total absorption to the star; whereas, for VY CMa, the circumstellar absorption likely dominates (Humphreys et al. 2007). The circumstellar absorption toward IRC+10420 provides an additional  $\sim 1$  mag of absorption — this modest extinction likely reflects our nearly pole-on view of the predominantly equatorial circumstellar material (Tiffany et al. 2010). Accounting for the likely absorbing column toward IRC +10420 (at least  $N_H \sim 10^{22}$  cm $^{-2}$  of interstellar and circumstellar absorption) and assuming a plasma temperature appropriate for coronal and self-shocking winds ( $T_X \sim 3 \times 10^6$  K), PIMMS simulations give the upper limit on the unabsorbed intrinsic X-ray flux from IRC+10420 as  $F_{X,\text{UL}} \lesssim 10^{-12}$  erg cm $^{-2}$  s $^{-1}$ . The upper limit on the relative X-ray luminosity then becomes  $L_X/L_{\text{bol}} \lesssim 10^{-6}$ . These rather modest constraints, relative to those we have obtained for VY CMa ( $F_{X,\text{UL}} \lesssim 8 \times 10^{-14}$  erg cm $^{-2}$  s $^{-1}$  and  $L_X/L_{\text{bol}} \lesssim 10^{-8}$ , respectively; §2.2), reflect in large part the low sensitivity of the XMM observations of IRC +10420 (this XMM exposure was only  $\sim 10$  ks in duration and was compromised by high particle backgrounds; De Becker et al. 2014).

Next, we compare the relative X-ray luminosities of VY CMa and IRC+10420 with those of the self-shocking winds of OB stars and W-R stars. Self-shocking winds of OB stars and W-R stars give rise to X-ray emission within the wind and typically feature plasmas of a few MK with  $L_X/L_{\text{bol}} \sim 10^{-7}$  (e.g., Nazé et al. 2011). These measurements are corrected for absorption by the ISM but not for additional self-absorption by the wind. Indeed, there is theoretical evidence that thin-shell mixing in O-star radiative wind shocks can lead to decreased  $L_X/L_{\text{bol}}$  ratios, especially in denser winds of earliest O types and W-R star winds (Owocki et al. 2013). Hence, caution is advised when making a comparison between OB stars and the red and yellow hypergiants considered here. Adopting the standard treatment of  $L_X$  measurements of OB stars and W-R stars, we consider the upper limit resulting from only interstellar extinction. For IRC+10420, most of the absorption arises from the ISM and  $L_X/L_{\text{bol}} \lesssim 10^{-6}$ , whereas for VY CMa, the cir-

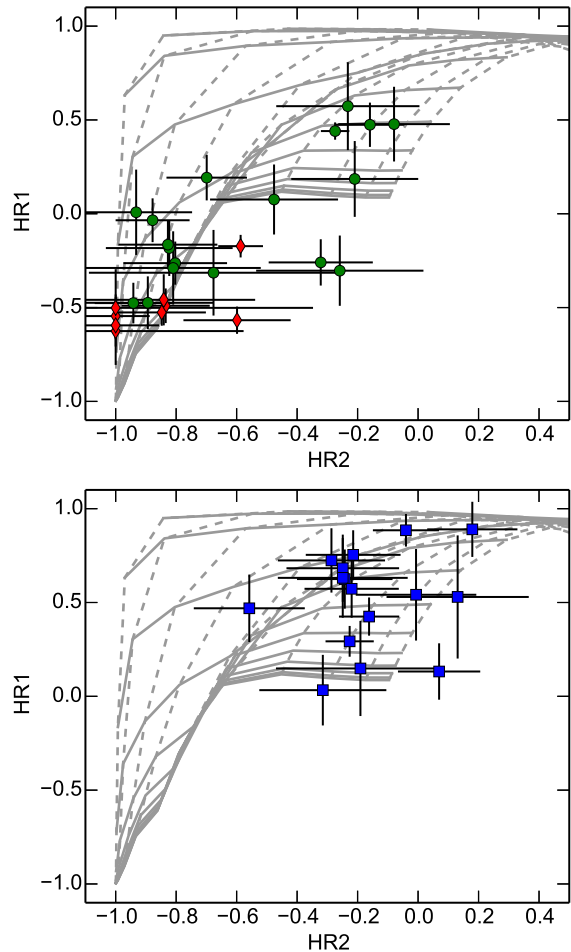


**Figure 5.** Hardness ratios of the strongest X-ray sources within  $15'$  of VY CMa. Symbols are as in Figure 3. X-ray emitting sources with IR counterparts are shown in the upper panel and those without IR counterparts are shown in the lower panel. A grid of absorbed, optically-thin thermal plasma models are overlaid as gray lines. The column densities from  $10^{20}$  to  $3 \times 10^{23}$  cm $^{-2}$  (solid lines) increase upwards while the plasma temperatures  $10^6$  to  $10^8$  K (dashed lines) increase from left to right.

cumstellar ejecta dominates the absorbing column to the star, so according to Figure 2 and an ISM column of  $\log N_H$  (cm $^{-2}$ )  $\sim 21.25$ ,  $L_X/L_{\text{bol}} \lesssim 10^{-9}$ . Such a low ratio suggests that VY CMa does not exhibit energetic (X-ray emitting) wind shocks in its ejecta. This result is not particularly surprising, given that its envelope terminal velocity is  $\sim 35$  km s $^{-1}$  (Humphreys et al. 2005), i.e., more than an order of magnitude lower than the typical wind speeds of hot, massive stars (whose wind speeds of hundreds to thousands of km s $^{-1}$  are compatible with X-ray-producing shocks). We caution that our observation of VY CMa is not sensitive to lower-speed (hence lower-temperature) shocks, which are more susceptible to absorption by circumstellar material (see Figure 2). On the other hand, after accounting for the ISM absorbing column toward IRC+10420, the XMM observations reported by De Becker et al. (2014) cannot constrain whether energetic shocks are present in the winds from IRC+10420 (whose envelope terminal velocity is  $\sim 70$  km s $^{-1}$ , Driebe et al. 2009).

**Table 1**  
X-ray Sources with IR counterparts

ID	RAJ2000 (decimal degrees)	DECJ2000 (decimal degrees)	$\theta_*^a$ (')	$\log F_X$ (erg cm <sup>-2</sup> s <sup>-1</sup> )	HR1	HR2	$\theta_{IR}^b$ (")	K (mag)	J-H (mag)	H-K (mag)
1	110.695236	-25.749485	2.8	-13.36	0.19	-0.21	4.8	14.47	0.21	0.10
2	110.681101	-25.795293	3.7	-13.58	-0.26	-0.32	4.6	13.32	0.64	0.20
3	110.827017	-25.832432	6.0	-13.14	0.47	-0.16	2.3	14.54	0.50	0.21
4	110.633655	-25.745552	6.1	-13.71	-0.48	-0.94	1.9	10.70	0.25	0.00
5	110.701152	-25.882938	7.3	-14.32	0.01	-0.93	1.7	13.87	0.66	0.16
6	110.919803	-25.802366	9.8	-13.44	-0.18	-0.82	2.8	13.07	0.52	0.15
7	110.576459	-25.688474	10.2	-13.42	0.48	-0.08	5.6	14.90	0.15	1.17
8	110.565065	-25.701433	10.4	-13.58	0.57	-0.23	4.9	14.67	0.75	0.06
9	110.551432	-25.726772	10.6	-13.67	-0.16	-0.83	1.3	12.66	0.39	0.11
10	110.546044	-25.777196	10.7	-13.82	-0.47	-0.89	0.9	10.38	0.35	0.12
11	110.706837	-25.586718	11.0	-14.14	-0.31	-0.68	1.2	13.46	0.65	0.11
12	110.577615	-25.657208	11.1	-13.47	-0.26	-0.80	1.7	12.78	0.62	0.21
13	110.561816	-25.677843	11.2	-12.34	0.44	-0.27	0.9	14.37	0.86	0.82
14	110.624613	-25.923327	11.3	-14.07	-0.29	-0.81	4.3	12.97	0.44	0.03
15	110.540498	-25.711559	11.5	-13.49	-0.03	-0.88	1.5	12.40	0.41	0.13
16	110.929428	-25.904013	13.0	-13.16	0.19	-0.70	3.7	11.40	0.39	0.10
17	110.743384	-25.986525	13.1	-13.74	-0.30	-0.26	3.0	13.75	0.65	0.22
18	111.018006	-25.802717	15.0	-13.59	0.08	-0.48	3.3	12.73	0.30	0.11

Sources with Measurable Proper Motion:

1	110.719126	-25.785464	1.7	-13.20	-0.17	-0.59	2.5	12.05	0.41	0.10
2	110.708815	-25.696935	4.6	-13.92	-0.55	-1.00	2.0	12.09	0.39	0.09
3	110.803036	-25.683911	6.0	-13.98	-0.50	-1.00	0.6	11.28	0.43	0.10
4	110.579420	-25.757902	8.9	-14.25	-0.63	-1.00	2.6	11.73	0.39	0.08
5	110.763456	-25.615153	9.2	-13.49	-0.49	-0.83	1.3	11.47	0.61	0.21
6	110.621950	-25.653632	9.5	-13.38	-0.53	-0.85	1.3	10.72	0.63	0.18
7	110.805101	-25.596622	10.8	-13.16	-0.57	-0.60	1.6	9.69	0.37	0.09
8	110.533127	-25.807030	11.6	-13.83	-0.46	-0.84	1.6	9.53	0.28	0.09
9	111.038003	-25.685400	16.7	-13.26	-0.59	-1.00	3.0	9.50	0.22	0.04

**Note.** — All measurements are observed and not dereddened.

<sup>a</sup> The offset angle between the X-ray source and the position of VY CMa.

<sup>b</sup> The offset angle between the X-ray source and the 2MASS source.

**Table 2**  
X-ray Sources without IR counterparts

ID	RAJ2000 (decimal degrees)	DECJ2000 (decimal degrees)	$\theta_*^a$ (')	$\log F_X$ (erg cm <sup>-2</sup> s <sup>-1</sup> )	HR1	HR2	$\theta_{IR}^b$ (")
1	110.712895	-25.765103	1.6	-13.17	0.43	-0.16	16
2	110.730628	-25.822038	3.3	-13.54	0.72	-0.29	14
3	110.804773	-25.807603	4.1	-13.01	0.29	-0.23	12
4	110.816902	-25.702447	5.6	-12.69	0.88	-0.04	17
5	110.703503	-25.864912	6.2	-13.46	0.68	-0.25	8.9
6	110.766224	-25.879853	6.9	-13.27	0.03	-0.31	11
7	110.615501	-25.768253	6.9	-13.65	0.47	-0.56	19
8	110.661126	-25.674120	7.1	-13.47	0.75	-0.21	16
9	110.871664	-25.801926	7.2	-13.36	0.62	-0.24	13
10	110.814463	-25.897295	8.7	-13.10	0.13	0.07	12
11	110.912240	-25.742049	9.3	-13.13	0.89	0.18	22
12	110.815658	-25.625267	9.4	-13.67	0.15	-0.19	8.7
13	110.717331	-25.591561	10.7	-13.57	0.54	-0.01	18
14	110.563373	-25.841295	10.7	-13.27	0.53	0.13	34
15	110.768536	-25.970898	12.3	-12.96	0.57	-0.22	18
16	110.742678	-25.973804	12.4	-13.35	0.63	-0.25	7.3

<sup>a</sup> The offset angle between the X-ray source and the position of VY CMa.

<sup>b</sup> The offset angle between the X-ray source and the nearest 2MASS catalog entry.

### 3.3. Constraints on a population of young stars associated with VY CMa

We now consider whether the X-ray sources we have detected in the field surrounding VY CMa might represent an associated group of lower-mass (late-type), pre-main sequence stars. In Figure 5, we compare the hardness ratios HR1 (soft & medium bands) and HR2 (medium & hard bands) of the 43 strongest X-ray sources to source model predictions. We considered an ab-

sorbed, solar-abundance, optically-thin thermal plasma model (MEKAL; Mewe et al. 1985, 1986; Kaastra 1992; Liedahl et al. 1995) characterized by an intervening absorbing column  $N_H$  and plasma temperature  $T_X$ . Our model grid is comprised of 15 logarithmically-spaced  $N_H$  values between  $10^{20}$  and  $3 \times 10^{23}$  cm<sup>-2</sup> and plasma model temperatures between  $10^6$  to  $10^8$  K. This model lacks the sophistication to classify the sources of X-ray emission, but helps establish approximate emission characteristics.



upper limit on  $L_X$ , we estimate that the surface-averaged magnetic field strength,  $fB$ , is less than  $10^{-3}$  G. Comparison with maser polarization measurements of magnetic field strengths throughout the ejecta of VY CMa, which imply surface magnetic field strengths as large as  $\sim 200$  G, suggests the filling factor of magnetically active regions on VY CMa ( $f$ ) was  $< 10^{-5}$  during the epoch of our observation. However, we stress that our XMM observations represent only a single-epoch snapshot of potential magnetic activity at VY CMa and hence, given the star's record of episodic high mass loss rate events, we may simply be observing the star during a lull between periods of enhanced surface activity.

We have detected more than 100 X-ray emitting sources within the  $\sim 30'$  diameter field of view of the XMM observation. The spatial distribution and hardness ratios of these X-ray sources suggest that many are affected by absorption within the molecular cloud associated with VY CMa, thus providing evidence that the sources themselves are at least at the distance of VY CMa. We have studied the 43 brightest X-ray sources via their hardness ratios and IR emission, and find that a subset may be late-type pre-MS stars potentially associated with VY CMa. The near-IR magnitudes and colors of roughly half of the 18 X-ray sources with IR counterparts are consistent with these stars being a young ( $\lesssim 10$  Myr-old) population that is similar in age and distance to the nearby cluster NGC 2362. Further study of this apparent group of young stars that is potentially associated with VY CMa may help constrain the age of the hypergiant itself.

#### Facilities: XMM (EPIC).

We acknowledge support from NASA Award Number, NNX13AB55G for our XMM observations of VY CMa. This research has made use of the NASA/ IPAC Infrared Science Archive, which is operated by the Jet Propulsion Laboratory, California Institute of Technology, under contract with the National Aeronautics and Space Administration. This publication makes use of data products from the Two Micron All Sky Survey, which is a joint project of the University of Massachusetts and the Infrared Processing and Analysis Center/California Institute of Technology, funded by the National Aeronautics and Space Administration and the National Science Foundation.

#### REFERENCES

- Ayres, T. R. 2005, *ApJ*, 618, 493  
 Ayres, T. R., Brown, A., & Harper, G. M. 2003, *ApJ*, 598, 610  
 Barvainis, R., McIntosh, G., & Predmore, C. R. 1987, *Nature*, 329, 613  
 Cohen, R. J., Downs, G., Emerson, R., et al. 1987, *MNRAS*, 225, 491  
 Damiani, F., Micela, G., Sciortino, S., et al. 2006, *A&A*, 460, 133  
 Danchi, W. C., Bester, M., Degiacomi, C. G., Greenhill, L. J., & Townes, C. H. 1994, *AJ*, 107, 1469  
 De Becker, M., Hutsemékers, D., & Gosset, E. 2014, *New Astronomy*, 29, 75  
 Driebe, T., Groh, J. H., Hofmann, K.-H., et al. 2009, *A&A*, 507, 301  
 Feiden, G. A., & Chaboyer, B. 2013, *ApJ*, 779, 183  
 Freeman, M., Montez, R., Jr, J. H. Kastner, et al. 2014, *arXiv:1407.4141*  
 Gilliland, R. L., & Dupree, A. K. 1996, *ApJ*, 463, L29  
 Herbig, G. H. 1972, *ApJ*, 172, 375  
 Humphreys, R. M., Davidson, K., Ruch, G., & Wallerstein, G. 2005, *AJ*, 129, 492  
 Humphreys, R. M., Davidson, K., & Smith, N. 2002, *AJ*, 124, 1026  
 Humphreys, R. M., Helton, L. A., & Jones, T. J. 2007, *AJ*, 133, 2716  
 Humphreys, R. M., Smith, N., Davidson, K., et al. 1997, *AJ*, 114, 2778  
 Kaastra, J.S. 1992, An X-Ray Spectral Code for Optically Thin Plasmas (Internal SRON-Leiden Report, updated version 2.0)  
 Karovska, M., Schlegel, E., Hack, W., Raymond, J. C., & Wood, B. E. 2005, *ApJ*, 623, L137  
 Kastner, J. H., Montez, R., Jr., Balick, B., et al. 2012, *AJ*, 144, 58  
 Kastner, J. H., & Soker, N. 2004b, *ApJ*, 616, 1188  
 Kastner, J. H., & Soker, N. 2004a, *ApJ*, 608, 978  
 Kastner, J. H., & Weintraub, D. A. 1998, *AJ*, 115, 1592  
 Jones, T. J., Humphreys, R. M., Helton, L. A., Gui, C., & Huang, X. 2007, *AJ*, 133, 2730  
 Jones, T. J., Humphreys, R. M., Gehrz, R. D., et al. 1993, *ApJ*, 411, 323  
 Lada, C. J., & Reid, M. J. 1978, *ApJ*, 219, 95  
 Liedahl, D. A., Osterheld, A. L., & Goldstein, W. H. 1995, *ApJ*, 438, L115  
 Meaburn, J., López, J. A., Boumis, P., Lloyd, M., & Redman, M. P. 2009, *A&A*, 500, 827  
 Mel'Nik, A. M., & Dambis, A. K. 2009, *MNRAS*, 400, 518  
 Mewe, R., Gronenschild, E. H. B. M., & van den Oord, G. H. J. 1985, *A&AS*, 62, 197  
 Mewe, R., Lemen, J. R., & van den Oord, G. H. J. 1986, *A&AS*, 65, 511  
 Moitinho, A., Alves, J., Huéamo, N., & Lada, C. J. 2001, *ApJ*, 563, L73  
 Monnier, J. D., Millan-Gabet, R., Tuthill, P. G., et al. 2004, *ApJ*, 605, 436  
 Montez, R., Jr., and ChanPlaNS collaboration, submitted  
 Montez, R., Jr., De Marco, O., Kastner, J. H., & Chu, Y.-H. 2010, *ApJ*, 721, 1820  
 Nazé, Y., Broos, P. S., Oskinova, L., et al. 2011, *ApJS*, 194, 7  
 O'Gorman, E., Vlemmings, W., Richards, A. M. S., et al. 2014, *arXiv:1410.1622*  
 Orlando, S., Peres, G., & Reale, F. 2004, *A&A*, 424, 677  
 Owocki, S. P., Sundqvist, J. O., Cohen, D. H., & Gayley, K. G. 2013, *MNRAS*, 429, 3379  
 Pevtsov, A. A., Fisher, G. H., Acton, L. W., et al. 2003, *ApJ*, 598, 1387  
 Parker, Q. A., Philipps, S., Pierce, M. J., et al. 2005, *MNRAS*, 362, 689  
 Posson-Brown, J., Kashyap, V. L., Pease, D. O., & Drake, J. J. 2006, *arXiv:astro-ph/0606387*  
 Ramstedt, S., Montez, R., Kastner, J., & Vlemmings, W. H. T. 2012, *A&A*, 543, A147  
 Schlegel, D. J., Finkbeiner, D. P., & Davis, M. 1998, *ApJ*, 500, 525  
 Skrutskie, M. F., Cutri, R. M., Stiening, R., et al. 2006, *AJ*, 131, 1163  
 Smith, N., Humphreys, R. M., Davidson, K., et al. 2001, *AJ*, 121, 1111  
 Stead, J. J., & Hoare, M. G. 2011, *MNRAS*, 418, 2219  
 Tiffany, C., Humphreys, R. M., Jones, T. J., & Davidson, K. 2010, *AJ*, 140, 339  
 Tuthill, P. G., Haniff, C. A., & Baldwin, J. E. 1997, *MNRAS*, 285, 529  
 Vlemmings, W. H. T., Diamond, P. J., & van Langevelde, H. J. 2002, *A&A*, 394, 589  
 Vlemmings, W. H. T., van Langevelde, H. J., & Diamond, P. J. 2005, *Mem. Soc. Astron. Italiana*, 76, 462  
 Watson, M. G., Schröder, A. C., Fyfe, D., et al. 2009, *A&A*, 493, 339  
 Wright, E. L., Eisenhardt, P. R. M., Mainzer, A. K., et al. 2010, *AJ*, 140, 1868  
 Zacharias, N., Finch, C. T., Girard, T. M., et al. 2013, *AJ*, 145, 44  
 Zhang, B., Reid, M. J., Menten, K. M., & Zheng, X. W. 2012, *ApJ*, 744, 23